The Journal of Chemical Physics

RESEARCH ARTICLE | OCTOBER 14 2019

Nanoelectrode-emitter spectral overlap amplifies surface enhanced electrogenerated chemiluminescence

Special Collection: Emerging Directions in Plasmonics

Thomas S. Heiderscheit ; Miranda J. Gallagher ; Rashad Baiyasi ; Sean S. E. Collins ; Seyyed Ali Hosseini Jebeli ; Leonardo Scarabelli ; Alexander Al-Zubeidi ; Charlotte Flatebo ; Wei-Shun Chang; Christy F. Landes ; Stephan Link

Check for updates

J. Chem. Phys. 151, 144712 (2019)
https://doi.org/10.1063/1.5118669
CHORUS

View Online
Export Citation

26 July 2024 15:52:13

AIP Publishing

The Journal of Chemical Physics
2024 Emerging Investigators Special Collection
Submit Today
AIP Publishing

The Journal of Chemical Physics ARTICLE scitation.org/journal/jcp

Nanoelectrode-emitter spectral overlap amplifies surface enhanced electrogenerated chemiluminescence

Cite as: J. Chem. Phys. 151, 144712 (2019); doi: 10.1063/1.5118669
Submitted: 5 July 2019 • Accepted: 16 September 2019 •
Published Online: 14 October 2019

View Online Export Citation CrossMark

Thomas S. Heiderscheit,[1] Miranda J. Gallagher,[1] Rashad Baiyasi,[2] Sean S. E. Collins,[1,3] Seyyed Ali Hosseini Jebeli,[2] Leonardo Scarabelli,[1,a)] Alexander Al-Zubeidi,[1] Charlotte Flatebo,[1,4] Wei-Shun Chang,[1,b)] Christy F. Landes,[1,2,c)] and Stephan Link[1,2,c)]

AFFILIATIONS

[1]Department of Chemistry, Rice University, 6100 Main Street, Houston, Texas 77005, USA
[2]Department of Electrical and Computer Engineering, Rice University, 6100 Main Street, Houston, Texas 77005, USA
[3]Smalley-Curl Institute, Rice University, 6100 Main Street, Houston, Texas 77005, USA
[4]Applied Physics Program, Rice University, 6100 Main Street, Houston, Texas 77005, USA

Note: The paper is part of the JCP Special Topic on Emerging Directions in Plasmonics.
[a)]**Present address:** California NanoSystems Institute, University of California Los Angeles, Los Angeles, CA 90095, USA.
[b)]**Present address:** Department of Chemistry and Biochemistry, University of Massachusetts Dartmouth, 285 Old Westport Rd., North Dartmouth, Massachusetts 02747, USA.
[c)]**Authors to whom correspondence should be addressed:** cflandes@rice.edu and slink@rice.edu

ABSTRACT

Electrogenerated chemiluminescence (ECL) is a promising technique for low concentration molecular detection. To improve the detection limit, plasmonic nanoparticles have been proposed as signal boosting antennas to amplify ECL. Previous ensemble studies have hinted that spectral overlap between the nanoparticle antenna and the ECL emitter may play a role in signal enhancement. Ensemble spectroscopy, however, cannot resolve heterogeneities arising from colloidal nanoparticle size and shape distributions, leading to an incomplete picture of the impact of spectral overlap. Here, we isolate the effect of nanoparticle-emitter spectral overlap for a model ECL system, coreaction of tris(2,2′-bipyridyl)dichlororuthenium(II) hexahydrate and tripropylamine, at the single-particle level while minimizing other factors influencing ECL intensities. We found a 10-fold enhancement of ECL among 952 gold nanoparticles. This signal enhancement is attributed exclusively to spectral overlap between the nanoparticle and the emitter. Our study provides new mechanistic insight into plasmonic enhancement of ECL, creating opportunities for low concentration ECL sensing.

Published under license by AIP Publishing. https://doi.org/10.1063/1.5118669

I. INTRODUCTION

Electrogenerated chemiluminescence (ECL) is a versatile analytical technique for detecting trace materials such as heavy metals in water,[1,2] the Zika virus in biological fluids,[3] and ketamine in hair.[4] ECL is the emission of light due to redox chemistry from applied external potentials, promoting an emitter to an excited state.[5,6] The intensity of emission from the excited state is proportional to the amount of analyte present. Compared to techniques such as Raman or fluorescence spectroscopy, ECL has relatively low background because external light is not required to drive emission. Recent ECL studies have focused on the synthesis of emitters with improved quantum yields and larger spectral tuning ranges,[7–10] discovery of novel applications,[11–13] and enhancement of the ECL signal.[14–16]

One promising method for ECL signal enhancement is coupling ECL emitters with gold nanoparticles.[15,17–22] The interaction of an emitter with a gold nanoparticle's coherent oscillation

26 July 2024 15:52:13

Published under license by AIP Publishing

of conduction band electrons, or localized surface plasmon resonance (LSPR),[23] leads to quenching and enhancement of ECL. While intensity enhancement occurs for Raman scattering,[24–26] both emitter enhancement and quenching are seen for fluorescence.[27–31] Surface enhanced electrogenerated chemiluminescence (SEECL) behaves similar to fluorescence.[32] Emitter quenching is in general attributed to fluorescence resonance energy transfer from the emitter to the nanoparticle,[33] while enhancement occurs through the modulation of the environment's local density of optical states.[27,34–37] Control of the spatial separation between the nanoparticle and the emitter minimizes ECL quenching and increases the ECL enhancement by the LSPR.[15,28] Quenching occurs at short distances (1–5 nm), while the enhancement maximizes at intermediate distances and then falls off again (5–20 nm).[15] Additionally, enhancement of ECL has shown dependence on nanoparticle shape[18] and on electric field hotspots at either sharp tips[21] or in the junctions of at least two nanoparticles.[20]

Early studies of SEECL relied primarily on ensemble techniques to observe the impact of the LSPR on ECL intensity.[15,17,18] Ensemble techniques cannot, however, resolve the heterogeneity in charge transfer, local environment, reactivity, or intrinsic differences in nanoparticle morphology in a spectroelectrochemical study of SEECL. This heterogeneity can be addressed with single particle techniques. Pan *et al.*[38] first used single particle spectroscopy to study SEECL driven on electrodeposited gold nanoparticles, observing not only heterogeneity in SEECL signal caused by nanoparticle size but heterogeneity of local conductivity in the indium tin oxide (ITO) coated substrate. The differences in conductivity resulted in a larger distribution of SEECL intensities from nanoparticles of the same size. Following this study, Wilson *et al.*[39] investigated the stability and activity of individual gold nanowires coated in a poly(3,4-ethylenedioxythiophene)-poly(styrenesulfonate) (PEDOT:PSS) and poly(vinyl alcohol) (PVA) polymer that prevented nanoparticle oxidation and dissolution. Finally, Zhu *et al.*[40] demonstrated heterogeneity in electrochemical activity between Au, Pt, and Au-Pt Janus nanoparticles. While no single particle study has reported the effect of spectral overlap, ensemble SEECL studies have inferred that the SEECL enhancement can be related to the spectral overlap between the nanoparticle scattering and the ECL spectra.[41,42] However, no single particle or ensemble SEECL studies, thus far, have comprehensively isolated the impact of spectral overlap by minimizing all other sources of heterogeneity in the system.

This work establishes a detailed study of nanoparticle-emitter spectral overlap in SEECL by measuring the variation in single particle dark-field scattering (DFS) spectra and SEECL intensities caused by changing nanoparticle shape and size. Gold nanospheres (AuNSs), with diameters between 72 and 112 nm, and gold nanotriangles (AuNTs), with edge lengths between 90 and 120 nm, were coated with PEDOT:PSS/PVA to protect against oxidation and dissolution.[43,44] Possible sources of heterogeneity in the system were minimized through background correction, using O_2 plasma cleaning, studying nanoparticles with similar crystal faceting, and normalizing for the surface area of individual nanoparticles. The SEECL intensities, expressed as photon flux, of 962 individual nanoparticles were then compared based on spectral overlap. A 10-fold enhancement of SEECL intensity was found for both AuNSs and AuNTs, where nanoparticles with larger spectral overlap showed stronger signal enhancement.

II. EXPERIMENTAL METHODS

A. Nanoparticle sample preparation and characterization

ITO coated glass coverslips (Evaporated Coatings Inc., ECI#949 56 Ω/sq., 22 × 22 mm) were sequentially sonicated in dilute detergent (Liquinox®), deionized (DI) water, acetone (Fisher Chemical, 99.7%), and DI water for 15 min each. Nanoparticles, either AuNSs (nanoComposix, 72 ± 26 nm and 99 ± 6 nm citrate capped and Nanopartz™, 82 ± 9 nm and 112 ± 28 nm citrate capped) or AuNTs (lab synthesized cetyltrimethylammonium chloride capped),[45] were spin cast (Laurel WS-650Mz-23BNPPB) onto coverslips that had been O_2 plasma cleaned for 2 min. The average diameters of the AuNSs and edge lengths of the AuNTs were measured with transmission electron microscopy (TEM) (Fig. S1). Ensemble sample quality was further confirmed with UV-Vis extinction spectroscopy (Fig. S1). AuNSs and AuNTs were selected to span a wide range of resonance wavelengths while minimizing effects arising from different crystal facets.[46,47] AuNSs have a primary crystal facet of {111},[48] while the AuNTs used also have a primary crystal facet of {111} for both the planar and lateral faces of the bifrustum geometry.[45]

B. Electrochemical cell preparation

120 μL of PEDOT:PSS (Sigma-Aldrich Co., 3.0%–4.0% in H_2O, high-conductive grade) was added to 680 μL of 3% (1.5 g/50 mL DI water) PVA (Sigma-Aldrich Co., M_W 146 000–186 000, 99+% hydrolyzed). A prepared nanoparticle/ITO sample was O_2 plasma cleaned for 2 min to remove surface ligands. Then, PEDOT:PSS/PVA was vortexed for 30 s[39] before spin casting onto the prepared nanoparticle/ITO sample at 500 RPM for 6 s followed by 3000 RPM for 60 s. Coverslips were dried on a hotplate at 100 °C and then the spin casting sequence was repeated. Samples were finally dried overnight in an oven at 60 °C before use. Polymer thickness was measured using profilometry (Veeco Dektak 6m) and found to be 380 nm (Fig. S2). The addition of the PEDOT:PSS/PVA polymer layer improved the reproducibility of ECL signal through slowing the diffusion of $Ru(bpy)_3^{2+}$ and decreasing the depletion of available $Ru(bpy)_3^{2+}$ at the gold nanoparticle surface.[39]

An electrochemical cell [Fig. 1(a)] was prepared with nanoparticle/ITO/PEDOT:PSS/PVA functioning as the working electrode (WE), platinum wire (Sigma-Aldrich Co., 0.076 mm) as the counter electrode (CE), and insulated platinum wire (A-M Systems, LLC., 0.002″ bare, 0.0040″ coated) as the quasi-reference electrode (RE). A clear and a red Silicone Isolator™ with SecureSeal adhesive (Grace Bio-Laboratories©, 1 mm) were used to separate the counterelectrode and working electrode and to hold the electrodes in place. The cell was then filled with an electrolyte solution containing the ECL active reagents of 2.5 mM tris(2,2′-bipyridyl)dichlororuthenium(II) hexahydrate (Sigma-Aldrich Co., 99.95%) [$Ru(bpy)_3^{2+}$] and 25 mM tripropylamine (Sigma-Aldrich Co., ≥98%) (TPA) in 7.4 pH phosphate buffer.[39,49,50] The filled cell was pressure sealed with a glass coverslip and aluminum plates and secured to the microscope stage.

26 July 2024 15:52:13

Published under license by AIP Publishing

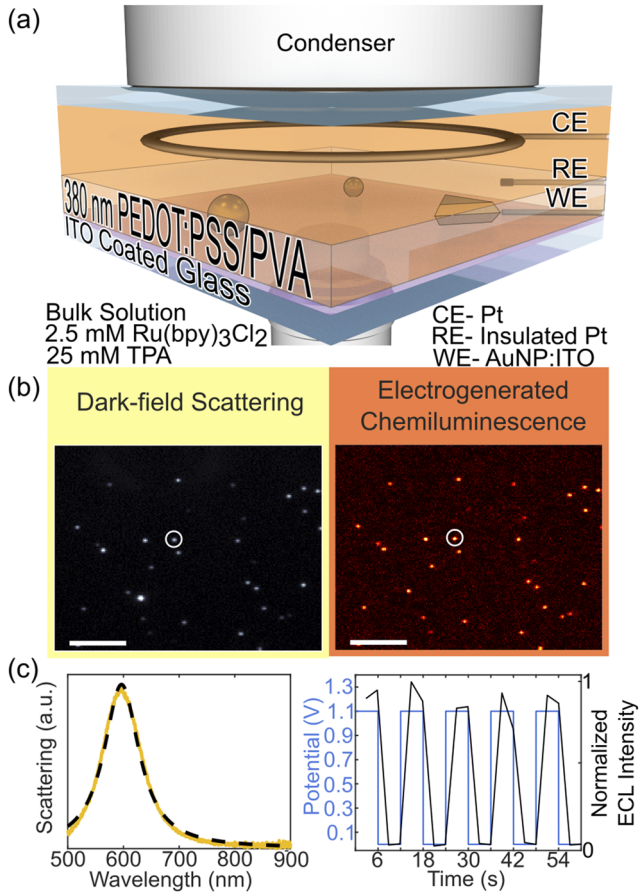

FIG. 1. Single particle SEECL spectroscopy. (a) DFS and SEECL of $Ru(bpy)_3^{2+}$ and PEDOT:PSS/PVA coated nanoparticles were measured separately using an electrochemical cell consisting of an nanoparticle/ITO working electrode (WE), Pt counter electrode (CE), and insulated Pt quasi-reference electrode (RE). (b) DFS (left) and single frame SEECL (right) images of 99 nm AuNSs were captured with a hyperspectral CCD camera and an EMCCD camera setup, respectively. Scale bar shown is 10 μm. (c) Single particle DFS spectrum (yellow, left), Lorentzian fit (dashed, left), and SEECL intensity time trace (black, right) of a representative nanoparticle [white circle in (b)]. The single particle DFS spectrum was fit with a Lorentzian function to extract peak resonance wavelength. SEECL was modulated using a square waveform from 0 to 1.1 V (blue, right) to turn ECL on and off.

C. Electrochemical DFS, SEECL, and ensemble $Ru(bpy)_3^{2+}$ emission measurements

DFS [Fig. 1(b), left] and SEECL [Fig. 1(b), right] were measured on an inverted microscope (Zeiss AxioObserver M1) using an oil immersion objective [Zeiss, PlanApochromat 63×, numerical aperture (NA) = 0.7]. The SEECL detection pathway consisted of an electron multiplying charge coupled device (EMCCD) camera (Andor, iXon Ultra 897). The DFS spectra were collected using a dark-field condenser (NA = 0.7–1.4), while the detection pathway consisted of a spectrograph (Princeton Instruments, SP2150i) equipped with a CCD camera (Princeton Instruments, PIXIS 400BR) mounted on a motorized translation stage.[51,52] During SEECL measurements, a three-electrode potentiostat (CH Instruments, 630 D) controlled potentials. While collecting SEECL on the EMCCD camera, the working electrode potential was varied with a custom LabVIEW (National Instruments) program.

Each SEECL measurement was acquired after a 30 min electrolyte incubation to allow for $Ru(bpy)_3^{2+}$ and TPA to replenish inside the polymer blend.[39] DFS spectra of gold nanoparticles were acquired during emitter and coreactant incubation with a 2 s integration time. Chronoamperometry was used to step the potential from 0 to 1.1 V with a pulse length of 6 s, repeated 10 times [Fig. 1(c), right]. The SEECL signal was measured with an integration time of 4 s for 72 and 82 nm AuNSs and 3 s for 99 nm AuNSs, 112 nm AuNSs, and AuNTs.

The raw $Ru(bpy)_3^{2+}$ SEECL images measured for AuNSs and AuNTs were converted into photon rates (counts per second). After a 1 h equilibration time, all frames when ECL was driven, i.e., applying 1.1 V, were summed to yield a photon rate. The conversion was accomplished by subtracting the background of $Ru(bpy)_3^{2+}$ ECL at the ITO surface and dividing by the integration time (4 or 3 s) and the total number of summed frames (Fig. S3). Measurements were started after a consistent ECL signal was obtained between measurements [Fig. S4(a)]. Signal reproducibility was achieved across different areas of a given electrochemical cell [Fig. S4(b)] and between individual electrochemical cells (Fig. S5). Single particle ECL intensity and DFS spectra were collected for 962 individual nanoparticles at a range of sizes and shapes (325 72 nm, 142 82 nm, 183 99 nm, and 135 112 nm AuNSs and 177 AuNTs).

Bulk $Ru(bpy)_3^{2+}$ emission was measured separately using the DFS detection pathway. A cell was constructed using an ITO coverslip in the same way as for SEECL experiments but without nanoparticles. The $Ru(bpy)_3^{2+}$ emission spectrum was collected with an integration time of 10 s and a slit width of 2 μm while applying 1.1 V.

D. Data analysis

DFS spectra [Fig. 1(c), solid yellow line, left] were fit to a Lorentzian function using a nonlinear least squares fitting algorithm (MATLAB 2018a) from which the nanoparticle peak resonance wavelengths were extracted [Fig. 1(c), dashed black line, left]. Only flat AuNTs were selected to reduce the heterogeneity in the ECL signal due to AuNT contact with the ITO surface, as differences in substrate contact could impact the charge transfer capability to the AuNT and to reduce possible polarization dependencies, as the dipole modes of the AuNTs are degenerate when lying flat. Because SEM could not resolve if the gold nanotriangles were lying flat, this selection was achieved by eliminating AuNTs with multiple scattering peaks (Fig. S6), demonstrated by Smith *et al.* to indicate an inclination in AuNTs.[53] Aggregates were also excluded from the analysis by rejecting spectra with maximum intensities more than twice the mean scattering intensity.

III. RESULTS AND DISCUSSION

Reproducible SEECL is observed when $Ru(bpy)_3^{2+}$ and TPA are coreacted on gold nanoparticles [Figs. 1(b) and 1(c)]. Under the electrochemical and reactant conditions used here, the ECL process described by Miao *et al.* is depicted in Steps 1–4 of Scheme 1.[6]

26 July 2024 15:52:13

Published under license by AIP Publishing

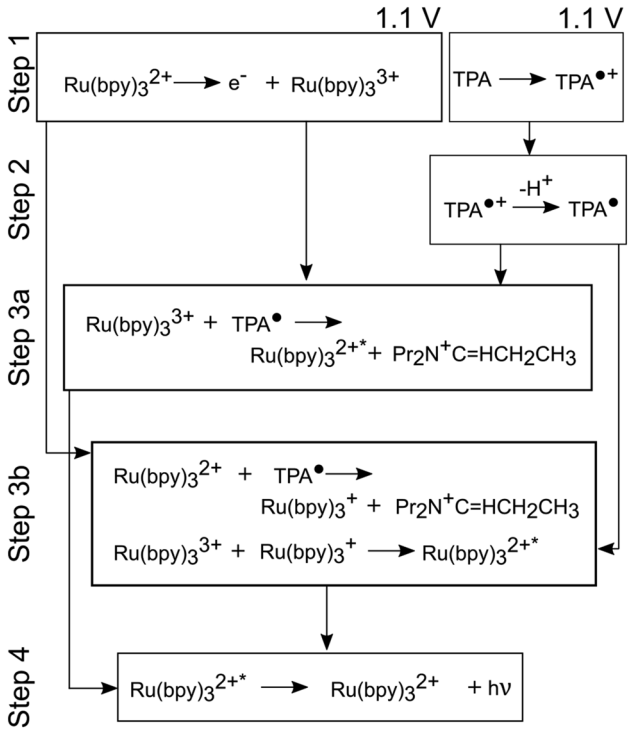

SCHEME 1. ECL reaction pathway for $Ru(bpy)_3^{2+}$ and TPA coreaction.

A potential of 1.1 V was used because 1.1 V is beyond not only the onset potential of $Ru(bpy)_3^{2+}$ and TPA oxidation [Figs. S7(a) and S7(b)], but also detectable ECL intensities [Fig. S7(c)], guaranteeing large ECL intensities.

There are several explanations in Scheme 1 for the SEECL in Fig. 1(b) at the gold nanoparticles relative to ECL at the ITO electrode surface. First, ITO has been shown to be weakly active for the oxidation of TPA in Step 1.[54] Gold nanoparticles, however, exhibit high TPA oxidation activity after modifying the nanoparticle surface through plasma cleaning[39,55] and preventing surface oxide passivation of the nanoparticle surface.[38,40,56] Differences in TPA oxidation activity, along with the plasmonic enhancement of $Ru(bpy)_3^{2+*}$ emission in Step 4,[32] resulted in the stronger ECL signal near the gold nanoparticles relative to ITO.

The PEDOT:PSS/PVA polymer ensured that $Ru(bpy)_3^{2+*}$ remained close to the surface of the AuNSs and the AuNTs through cation exchange.[50] Though distances likely varied significantly, emitters within 1–5 nm experienced quenching due to energy transfer from the emitter to the plasmon,[57] while emitters 5–20 nm from the nanoparticle surface were enhanced due to the modulation in the local density of optical states.[57] To estimate the reach of $Ru(bpy)_3^{2+}$ oxidation reaction from the electrode, the current data from the ECL experiments were used to calculate a concentration profile of $Ru(bpy)_3^{2+}$ and diffusion layer thickness after 6 s of potential polarization (Fig. S8). The diffusion layer thickness was found to be 30 μm, confirming that there should be emitters within the quenching and enhancement region. Because we did not control nanoparticle–emitter distances here, the measured SEECL signal represents an average over both quenching and enhancement. We assume a similar averaging for all nanoparticle samples. Both ECL quenching and enhancement should increase with a larger spectral overlap,[58–60] directly impacting the observed photon rate dependent on whether quenching or enhancement is more dominant.

SEECL intensities increased as the AuNS diameter increased, as demonstrated by the photon rate images shown in the left column of Fig. 2. A combination of AuNSs of different diameters [Figs. 2(a)–2(d)] and AuNTs [Fig. 2(e)] of different edge lengths provided a range of LSPRs that sampled across the entire emission spectrum of $Ru(bpy)_3^{2+}$ from 563 to 646 nm for AuNSs and from 585 to 799 nm for AuNTs, while the ECL peaked at 624 nm. Specifically, as the AuNS diameter increased, the AuNS peak resonance wavelength shifted toward the $Ru(bpy)_3^{2+}$ emission peak wavelength resulting in a higher spectral overlap, represented in the right column of Fig. 2 by the difference in peak wavelength ($\Delta\lambda_{max}$) between the nanoparticle scattering and $Ru(bpy)_3^{2+}$ emission spectra.

In addition to the increase in spectral overlap, the surface area of the AuNSs also increases with larger AuNS diameters. Nanoparticles with larger surface areas have a higher number of $Ru(bpy)_3^{2+}$ and TPA molecules nearby, resulting in a higher $Ru(bpy)_3^{2+}$ emission intensity compared to nanoparticles with smaller surface areas.[38] Because spectral overlap and surface area both change in the same direction, with an increase in nanoparticle diameter leading to more ECL photons collected per collection window, the photon rate images in Fig. 2 are not sufficient to directly isolate the impact of spectral overlap on ECL intensity.

Unlike the AuNSs, the impacts of $\Delta\lambda_{max}$ and surface area for AuNTs are more noticeable due to the inverse relationship between the surface area and $\Delta\lambda_{max}$ for AuNTs. The single particle DFS correlated photon rates of 785 AuNSs and 177 AuNTs were compared to the $Ru(bpy)_3^{2+}$ emission spectrum to track photon rate as both surface area and $\Delta\lambda_{max}$ change (Fig. 3). As the AuNS resonance wavelength approached the $Ru(bpy)_3^{2+}$ emission wavelength ($\Delta\lambda_{max} = 0$), the photon rate increased, which correlated with an increase in the surface area. Similarly, for AuNTs, the photon rate increased as $\Delta\lambda_{max}$ decreased. The increased photon rate did not correlate with an increased AuNT surface area because as the AuNT edge length increased, the resonance wavelength red shifted and $\Delta\lambda_{max}$ increased [Fig. S9(a)].[61,62] If the photon rate for AuNTs was solely dependent on surface area, then the opposite trend would be expected. Therefore, the observed $\Delta\lambda_{max}$ dependent trend confirmed that plasmonic enhancement dominated relative to the decreased number of emitters as the AuNT surface area decreased.

To control for differences in surface area, or number of nearby emitters, on SEECL, the photon rate was normalized by the corresponding surface area through correlating surface area with the resonance wavelength. Note that correlated SEM was not possible with these electrochemical devices because of the PEDOT:PSS/PVA polymer. We used Mie theory to model the relationship between the AuNS diameter and resonance wavelength (Fig. S10).[63] The established diameter and wavelength relationship was then converted to a dependence of surface area on resonance wavelength and further corrected for possible loss of surface area at the AuNS base (see the supplementary material for details). Mie theory could not be used to model the relationship between the AuNT edge length

26 July 2024 15:52:13

Published under license by AIP Publishing

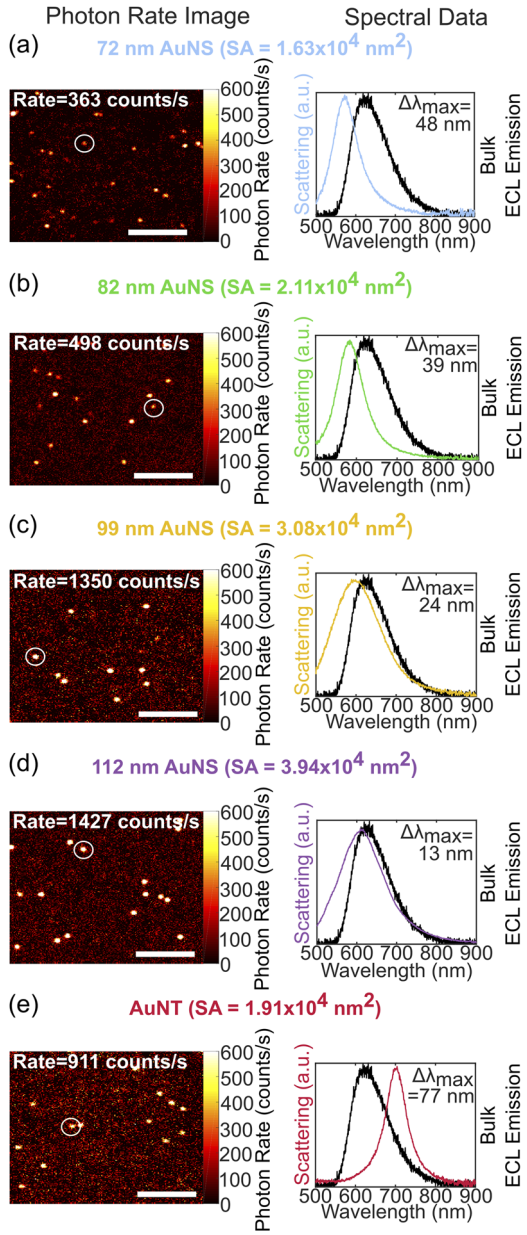

FIG. 2. Representative SEECL photon rate images (left) and single nanoparticle DFS spectra (right) for (a) 72 (light blue), (b) 82 (green), (c) 99 (yellow), (d) 112 (purple) nm AuNSs, and (e) AuNTs (red). The $Ru(bpy)_3^{2+}$ emission spectrum (black) is also shown. The surface areas shown in (a)–(e) are the total surface areas for each nanoparticle size and shape. Scale bar corresponds to 2 μm. Photon rate is scaled the same way between all images to allow for visual comparison. The photon rate given by the white text in the image and the single particle DFS spectrum are from the specific nanoparticle indicated by the white circle in each panel.

and resonance wavelength because Mie theory does not model nonspherical particles.[63] This link was instead established experimentally through DFS and SEM correlation for AuNTs not imbedded in PEDOT:PSS/PVA and found to be linear [Fig. S9(a)], consistent

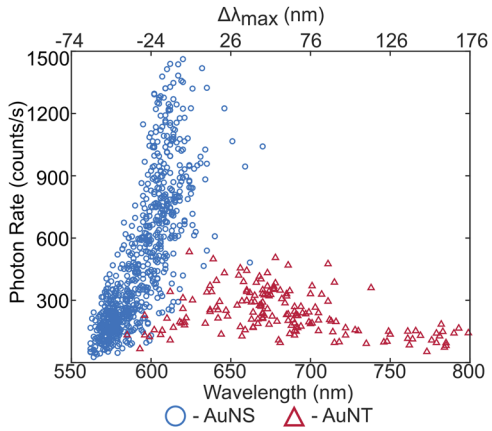

FIG. 3. Photon rate dependence on resonance wavelength and $\Delta\lambda_{max}$ for AuNSs (blue, circles) and AuNTs (red, triangles). $\Delta\lambda_{max}$ = 0 for 624 nm corresponding to the emission maximum of the $Ru(bpy)_3^{2+}$ ECL spectrum.

with previous reports.[61,62,64] Considering the resonance shift between AuNTs with and without PEDOT:PSS/PVA [Figs. S9(c) and S9(d)], the surface area of the AuNTs could then be determined using the known bifrustum geometry shown in Fig. S9(b), excluding the bottom surface due to contact with the ITO substrate.[53] As a result, the plasmon resonance wavelength allowed us to assign the surface area for each individual nanoparticle and to convert from the photon rate (counts per second) to photon flux [count/s nm^2], effectively removing the impact of the number concentration of emitters on the SEECL intensity. The resulting photon flux dependence on the resonance wavelength and $\Delta\lambda_{max}$ is illustrated in Fig. 4(a) for all nanoparticles investigated. The $\Delta\lambda_{max}$ dependent trend for AuNS and AuNT photon fluxes exhibited a similar shape to the $Ru(bpy)_3^{2+}$ emission spectrum after scaling the SEECL to the average photon flux at the $Ru(bpy)_3^{2+}$ emission peak at 624 nm. Both nanostructures had approximately a 10 times enhancement of photon flux as $\Delta\lambda_{max}$ decreased and approached zero, calculated by averaging the lowest and highest 20 data points for each shape in Fig. 4(a). The photon flux trend demonstrated that the smallest $\Delta\lambda_{max}$ caused the largest SEECL intensity for both AuNSs and AuNTs.

When factors that influence SEECL other than spectral overlap were minimized, a positive correlation between the spectral overlap and SEECL is observed in Fig. 4(b) and was not shape dependent. Spectral overlap was quantified by taking the ratio of integrated overlap between the normalized single particle DFS spectrum and the ensemble $Ru(bpy)_3^{2+}$ emission spectrum to the integral of the entire emission spectrum (Fig. S11). For AuNSs and AuNTs, photon flux was enhanced by 2.3 ± 1.3 times and 3.2 ± 2.3 times, respectively, when increasing the spectral overlap from 0.3 to 0.7 (Fig. S12). The lack of shape dependence is contrary to previously reported studies.[21] The AuNTs are expected to have a higher enhancement due to larger local electric fields at their tips. However, the AuNTs used in these experiments had dull tips (Fig. S1), resulting in weaker electric fields and lower SEECL relative to AuNTs with sharp tips.[65,66] Further considering that the AuNSs and AuNTs used here had the same primary crystal facet of {111},[45,48] the observed shape independence can be understood.

26 July 2024 15:52:13

Published under license by AIP Publishing

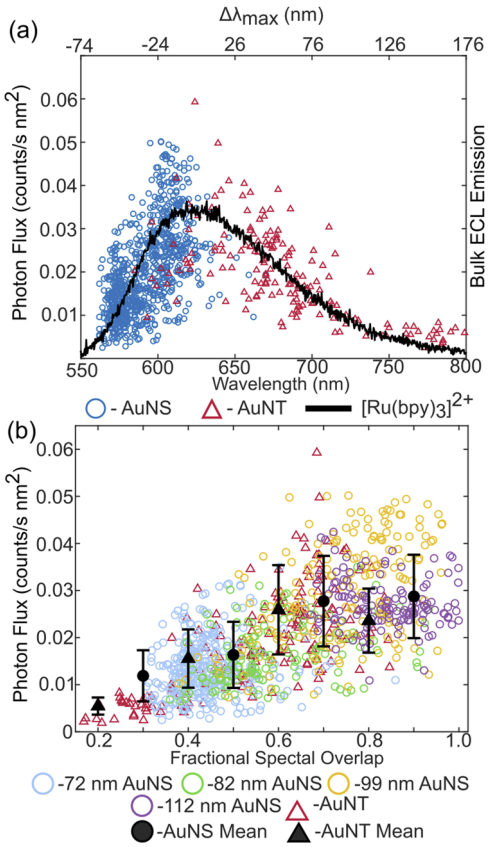

FIG. 4. Shape dependent $Ru(bpy)_3^{2+}$ SEECL photon flux and nanoparticle–emitter spectral overlap. (a) Photon flux dependence on the peak resonance wavelength for AuNSs (blue, circles) and AuNTs (red, triangles) overlaid on the scaled $Ru(bpy)_3^{2+}$ emission spectrum. (b) Photon flux dependence on normalized spectral overlap for 72 (light blue, circles), 82 (gray, circles), 99 (yellow, circles), and 112 (purple, circles) nm AuNSs and AuNTs (red, triangles) where the spectral overlap is defined as the area between the $Ru(bpy)_3^{2+}$ emission spectrum and each single nanoparticle DFS spectrum. This spectral overlap was calculated with the method illustrated in Fig. S12. The black circles and triangles with error bars represent the binned mean and standard deviation of photon flux for a wavelength interval of 10 nm. For clarity, mean values are shown for every other 10 nm step to distinguish between AuNSs (black, circles) and AuNTs (black, triangles). See Fig. S12 for the complete data set. $\Delta\lambda_{max} = 0$ is defined as in Fig. 3.

While the photon fluxes matched the ECL spectrum well, the largest AuNSs in Fig. 4(a) deviated giving higher values. This discrepancy can be explained when considering that the surface area is only an approximation. $Ru(bpy)_3^{2+}$ emission was quenched and enhanced over the sensing volume of each nanoparticle, i.e., in a shell around the nanoparticle surface. The thickness of this shell increased with increasing nanoparticle size as the electric field strength decreases roughly exponentially away from the surface with a decay length proportional to the nanoparticle radius.[67] Larger AuNSs, therefore, had larger sensing volumes, not accounted for when normalizing by the surface area alone, while AuNTs had electric field distributions more localized at the tips, not accounted for in our analysis. Considering that we did not control nanoparticle-emitter distances and hence recorded SEECL intensities averaged over many $Ru(bpy)_3^{2+}$ molecules at different positions, normalization by surface areas is a reasonable approximation, instead of correction with simulated sensing volumes.

Another source of heterogeneity observed in the literature previously,[38,68] local variations of the conductivity of the ITO substrate and especially the contact with the gold nanoparticles, could not be removed in this study but appears to have little effect. A difference in conductivity would result in different ECL intensities between similarly sized nanoparticles on the same ITO substrate. However, error propagation of the AuNS diameter and hence surface area (Figs. S10(c) and S10(d)] almost completely account for the spread in photon flux seen in Fig. 4(a). Therefore, we must conclude that heterogeneous conductivity could still have some impact on the measured SEECL data, but this effect is small in comparison with the variation in nanoparticle size.

IV. CONCLUSIONS

In summary, we carried out a comprehensive study of the impact of spectral overlap on the enhancement of ECL for the entire $Ru(bpy)_3^{2+}$ emission spectrum while minimizing the effects of other sources of ECL intensity heterogeneity. Increasing the spectral overlap between the nanoparticle DFS spectrum and the $Ru(bpy)_3^{2+}$ emission spectrum enhanced the single particle SEECL of $Ru(bpy)_3^{2+}$ up to 10 times. AuNSs and AuNTs, when corrected for surface area, demonstrated statistically similar spectral overlap dependences. The similar dependences indicated that there was no effect of shape for SEECL. We attribute this result to the dull tips of the AuNTs and both nanoparticle shapes having the same crystal facets. In order to maximize the absolute SEECL signal, structures need both a large surface area, to allow for higher emitter concentration within the enhancement region, and a fractional spectral overlap close to unity.

SUPPLEMENTARY MATERIAL

See supplementary material for TEM, UV-Vis extinction, and size distributions of AuNSs and AuNTs, profilometry of PEDOT:PSS/PVA, analysis method of raw ECL data, reproducibility of the signal over time and multiple areas or cells, polarization studies of AuNTs, electrochemical characterization, emitter concentration calculation, surface area correlation with the resonance wavelength of AuNTs, surface area correlation with the resonance wavelength of AuNSs, fractional spectral overlap calculation, and photon flux enhancement.

ACKNOWLEDGMENTS

This work was primarily supported by the U.S. Department of Energy, Office of Science, Basic Energy Sciences, CPIMS Program under Award No. DE-339SC0016534. We also acknowledge funding from the Robert A. Welch Foundation (Grant No. C-340 1787 to C.F.L., Grant No. C-1664 to S.L.). S.S.E.C. acknowledges support from the Smalley-Curl Institute at Rice University through a Carl and Lillian Illig Fellowship. C.F. acknowledges support from a National Defense Science and Engineering Graduate Fellowship. This work was conducted in part using resources of the Shared Equipment Authority at Rice University.

26 July 2024 15:52:13

Published under license by AIP Publishing

REFERENCES

[1] M. Zhang, L. Ge, S. Ge, M. Yan, J. Yu, J. Huang, and S. Liu, Biosens. Bioelectron. **41**, 544 (2013).
[2] G. Aragay and A. Merkoçi, Electrochim. Acta **84**, 49 (2012).
[3] D. Acharya, P. Bastola, L. Le, A. M. Paul, E. Fernandez, M. S. Diamond, W. Miao, and F. Bai, Sci. Rep. **6**, 32227 (2016).
[4] Y. Yang, S. Zhai, C. Liu, X. Wang, and Y. Tu, ACS Omega **4**, 801 (2019).
[5] A. J. Bard, *Electrogenerated Chemiluminescence* (Marcel Dekker, New York, 2004).
[6] W. Miao, J.-P. Choi, and A. J. Bard, J. Am. Chem. Soc. **124**, 14478 (2002).
[7] J. I. Kim, I.-S. Shin, H. Kim, and J.-K. Lee, J. Am. Chem. Soc. **127**, 1614 (2005).
[8] M. Zhou, G. P. Robertson, and J. Roovers, Inorg. Chem. **44**, 8317 (2005).
[9] J. McCall, D. Bruce, S. Workman, C. Cole, and M. M. Richter, Anal. Chem. **73**, 4617 (2001).
[10] L. C. Soulsby, D. J. Hayne, E. H. Doeven, D. J. D. Wilson, J. Agugiaro, T. U. Connell, L. Chen, C. F. Hogan, E. Kerr, J. L. Adcock, P. S. Donnelly, J. M. White, and P. S. Francis, Phys. Chem. Chem. Phys. **20**, 18995 (2018).
[11] H. C. Moon, T. P. Lodge, and C. D. Frisbie, J. Am. Chem. Soc. **136**, 3705 (2014).
[12] H. C. Moon, T. P. Lodge, and C. D. Frisbie, J. Mater. Chem. C **4**, 8448 (2016).
[13] S. Kirschbaum-Harriman, M. Mayer, A. Duerkop, T. Hirsch, and A. J. Baeumner, Analyst **142**, 2469 (2017).
[14] G. Jie, L. Li, C. Chen, J. Xuan, and J.-J. Zhu, Biosens. Bioelectron. **24**, 3352 (2009).
[15] Y. Shan, J.-J. Xu, and H.-Y. Chen, Chem. Commun. **45**, 905 (2009).
[16] S. Kirschbaum-Harriman, A. Duerkop, and A. J. Baeumner, Analyst **142**, 2648 (2017).
[17] J. Wang, Y. Shan, W.-W. Zhao, J.-J. Xu, and H.-Y. Chen, Anal. Chem. **83**, 4004 (2011).
[18] H. Zhou, Y.-Y. Zhang, J. Liu, J.-J. Xu, and H.-Y. Chen, J. Phys. Chem. C **116**, 17773 (2012).
[19] Y.-Y. Zhang, Q.-M. Feng, J.-J. Xu, and H.-Y. Chen, ACS Appl. Mater. Interfaces **7**, 26307 (2015).
[20] M.-X. Li, W. Zhao, G.-S. Qian, Q.-M. Feng, J.-J. Xu, and H.-Y. Chen, Chem. Commun. **52**, 14230 (2016).
[21] M.-X. Li, Q.-M. Feng, Z. Zhou, W. Zhao, J.-J. Xu, and H.-Y. Chen, Anal. Chem. **90**, 1340 (2018).
[22] H.-J. Lu, J.-B. Pan, Y.-Z. Wang, S.-Y. Ji, W. Zhao, X.-L. Luo, J.-J. Xu, and H.-Y. Chen, Anal. Chem. **90**, 10434 (2018).
[23] G. V. Hartland, Chem. Rev. **111**, 3858 (2011).
[24] P. L. Stiles, J. A. Dieringer, N. C. Shah, and R. P. Van Duyne, Annu. Rev. Anal. Chem. **1**, 601 (2008).
[25] C. E. Talley, J. B. Jackson, C. Oubre, N. K. Grady, C. W. Hollars, S. M. Lane, T. R. Huser, P. Nordlander, and N. J. Halas, Nano Lett. **5**, 1569 (2005).
[26] E. L. Keller and R. R. Frontiera, ACS Nano **12**, 5848 (2018).
[27] Y. Fu, J. Zhang, and J. R. Lakowicz, J. Am. Chem. Soc. **132**, 5540 (2010).
[28] A. S. De Silva Indrasekara, B. Shuang, F. Hollenhorst, B. S. Hoener, A. Hoggard, S. Chen, E. Villarreal, Y.-Y. Cai, L. Kisley, P. J. Derry, W.-S. Chang, E. R. Zubarev, E. Ringe, S. Link, and C. F. Landes, J. Phys. Chem. Lett. **8**, 299 (2017).
[29] A. Bek, R. Jansen, M. Ringler, S. Mayilo, T. A. Klar, and J. Feldmann, Nano Lett. **8**, 485 (2008).
[30] W. Zhang, M. Caldarola, X. Lu, B. Pradhan, and M. Orrit, Phys. Chem. Chem. Phys. **20**, 20468 (2018).
[31] N. Zou, G. Chen, X. Mao, H. Shen, E. Choudhary, X. Zhou, and P. Chen, ACS Nano **12**, 5570 (2018).
[32] D. Wang, L. Guo, R. Huang, B. Qiu, Z. Lin, and G. Chen, Sci. Rep. **5**, 7954 (2015).
[33] J.-F. Li, C.-Y. Li, and R. F. Aroca, Chem. Soc. Rev. **46**, 3962 (2017).
[34] R. Regmi, A. A. Al Balushi, H. Rigneault, R. Gordon, and J. Wenger, Sci. Rep. **5**, 15852 (2015).
[35] P. Bharadwaj and L. Novotny, Opt. Express **15**, 14266 (2007).
[36] J. R. Lakowicz, Anal. Biochem. **337**, 171 (2005).
[37] F. Tam, G. P. Goodrich, B. R. Johnson, and N. J. Halas, Nano Lett. **7**, 496 (2007).
[38] S. Pan, J. Liu, and C. M. Hill, J. Phys. Chem. C **119**, 27095 (2015).
[39] A. J. Wilson, K. Marchuk, and K. A. Willets, Nano Lett. **15**, 6110 (2015).
[40] M.-J. Zhu, J.-B. Pan, Z.-Q. Wu, X.-Y. Gao, W. Zhao, X.-H. Xia, J.-J. Xu, and H.-Y. Chen, Angew. Chem., Int. Ed. **57**, 4010 (2018).
[41] D. Wang, L. Guo, R. Huang, B. Qiu, Z. Lin, and G. Chen, Electrochim. Acta **150**, 123 (2014).
[42] P. Perez-Tejeda, E. Grueso, A. Marin-Gordillo, C. Torres-Marquez, and R. M. Giráldez-Pérez, ACS Appl. Nano Mater. **1**, 5307 (2018).
[43] H. Minamimoto, S. Oikawa, T. Hayashi, A. Shibazaki, X. Li, and K. Murakoshi, J. Phys. Chem. C **122**, 14162 (2018).
[44] T. Sannomiya, H. Dermutz, C. Hafner, J. Vörös, and A. B. Dahlin, Langmuir **26**, 7619 (2010).
[45] L. Scarabelli, M. Coronado-Puchau, J. J. Giner-Casares, J. Langer, and L. M. Liz-Marzán, ACS Nano **8**, 5833 (2014).
[46] Q. Zhang, L. Han, H. Jing, D. A. Blom, Y. Lin, H. L. Xin, and H. Wang, ACS Nano **10**, 2960 (2016).
[47] L. Sun, Q. Zhang, G. G. Li, E. Villarreal, X. Fu, and H. Wang, ACS Nano **11**, 3213 (2017).
[48] Y. Tang and W. Cheng, Langmuir **29**, 3125 (2013).
[49] R. M. Wightman, S. P. Forry, R. Maus, D. Badocco, and P. Pastore, J. Phys. Chem. B **108**, 19119 (2004).
[50] C. Sun, W. Lu, Y. Gao, and J. Li, Anal. Chim. Acta **632**, 163 (2009).
[51] B. S. Hoener, C. P. Byers, T. S. Heiderscheit, A. S. De Silva Indrasekara, A. Hoggard, W.-S. Chang, S. Link, and C. F. Landes, J. Phys. Chem. C **120**, 20604 (2016).
[52] C. P. Byers, B. S. Hoener, W.-S. Chang, M. Yorulmaz, S. Link, and C. F. Landes, J. Phys. Chem. B **118**, 14047 (2014).
[53] K. W. Smith, J. Yang, T. Hernandez, D. F. Swearer, L. Scarabelli, H. Zhang, H. Zhao, N. A. Moringo, W.-S. Chang, L. M. Liz-Marzán, E. Ringe, P. Nordlander, and S. Link, J. Phys. Chem. C **122**, 13259 (2018).
[54] Z. Chen and Y. Zu, Langmuir **23**, 11387 (2007).
[55] Y. Zu and A. J. Bard, Anal. Chem. **73**, 3960 (2001).
[56] Y. Zu and A. J. Bard, Anal. Chem. **72**, 3223 (2000).
[57] M. Li, S. K. Cushing, and N. Wu, Analyst **140**, 386 (2015).
[58] M. P. Singh and G. F. Strouse, J. Am. Chem. Soc. **132**, 9383 (2010).
[59] M. Olejnik, L. Bujak, and S. Mackowski, Int. J. Mol. Sci. **13**, 1018 (2012).
[60] Y. Chen, K. Munechika, and D. S. Ginger, Nano Lett. **7**, 690 (2007).
[61] M. R. Langille, M. L. Personick, J. Zhang, and C. A. Mirkin, J. Am. Chem. Soc. **134**, 14542 (2012).
[62] E. Ringe, M. R. Langille, K. Sohn, J. Zhang, J. Huang, C. A. Mirkin, R. P. Van Duyne, and L. D. Marks, J. Phys. Chem. Lett. **3**, 1479 (2012).
[63] C. F. Bohren, and D. R. Huffman, *Absorption and Scattering of Light by Small Particles* (John Wiley & Sons, Mörlenbach, Germany, 1983).
[64] N. Félidj, J. Grand, G. Laurent, J. Aubard, G. Lévi, A. Hohenau, N. Galler, F. R. Aussenegg, and J. R. Krenn, J. Chem. Phys. **128**, 094702 (2008).
[65] A. L. Demming, F. Festy, and D. Richards, J. Chem. Phys. **122**, 184716 (2005).
[66] D. A. Rosen and A. R. Tao, ACS Appl. Mater. Interfaces **6**, 4134 (2014).
[67] M. E. Stewart, C. R. Anderton, L. B. Thompson, J. Maria, S. K. Gray, J. A. Rogers, and R. G. Nuzzo, Chem. Rev. **108**, 494 (2008).
[68] Y.-H. Liau, N. F. Scherer, and K. Rhodes, J. Phys. Chem. B **105**, 3282 (2001).

26 July 2024 15:52:13

Published under license by AIP Publishing